ELSEVIER

Clinical Neurophysiology 110 (1999) 604–614

Common spatial subspace decomposition applied to analysis of brain responses under multiple task conditions: a simulation study

Yunhua Wang[a, b], Patrick Berg[c], Michael Scherg[a,*]

[a]*Department of Neurology, University of Heidelberg, Heidelberg, Germany*
[b]*Department of Electrical Engineering, Tsinghua University, Beijing, People's Republic of China*
[c]*Department of Psychology, University of Konstanz, Konstanz, Germany*

Accepted 30 September 1998

Abstract

A method, called common spatial subspace decomposition, is presented which can extract signal components specific to one condition from multiple magnetoencephalography/electroencephalography data sets of multiple task conditions. Signal matrices or covariance matrices are decomposed using spatial factors common to multiple conditions. The spatial factors and corresponding spatial filters are then dissociated into specific and common parts, according to the common spatial subspace which exists among the data sets. Finally, the specific signal components are extracted using the corresponding spatial filters and spatial factors. The relationship between this decomposition and spatio-temporal source models is described in this paper. Computer simulations suggest that this method can facilitate the analysis of brain responses under multiple task conditions and merits further application.

Keywords: Magnetoencephalography/electroencephalography; Evoked responses; Multiple cognitive tasks; Spatio-temporal dipole model; Common spatial subspace decomposition; Covariance matrix analysis

1. Introduction

For many decades, electrophysiological studies of the functional organization of the human brain had been limited to invasive measurements of the electrical potentials recorded from the cortical surface or from deep electrodes placed into the brain during surgical exploration in patients. In the past few years, non–invasive measurements of human brain function become increasingly attractive. Such measurements often use various kinds of sensory stimuli, or cognitive tasks to measure higher brain functions. Because spontaneous brain activity and non–task related activities overlap with the task related activities, one of the key problems in such measurements is how to separate these activities.

In most studies using positron emission topography (PET) or functional magnetic resonance imaging (fMRI), experimental paradigms are carefully designed to extract only the desired task related (target) activities. A common example of such a paradigm contains two kinds of stimuli: a target stimulus and a control stimulus. The target stimulus elicits the specific task related cortical activities, as well as other stimulus-related activities. The control stimulus elicits only these latter activities. Target activities, for example, statistical maps, can be extracted by calculating the difference between images measured with each kind of stimulus.

Although PET and fMRI can provide very high spatial resolution, they have a very limited temporal resolution compared to magnetoencephalography (MEG) (Hämäläinen et al., 1993) and electroencephalography (EEG) (Nunez, 1981). Since brain areas usually become activated within milliseconds during sensory discriminations and motor control, MEG/EEG are the only non-invasive techniques which can resolve the sequence and temporal relationship of the activation patterns in various brain areas involved in a specific sensory, motor or cognitive task. Indeed, many MEG/EEG measurements have been used to analyze brain functions (e.g. Scherg and von Cramon, 1985, 1986; Sasaki et al., 1989; Scherg, 1990; Scherg and Picton, 1991; Lehmann et al., 1994; Aine et al., 1995; Elbert et al., 1995; Beisteiner et al., 1996; Gevins et al., 1996; Rossini et al., 1996; Srebro and Ogui, 1997). However, analysis of experiments using task and control stimuli is impeded by the fact that appropriate analysis methods are not yet available to discern among conditions.

* Corresponding author. Tel.: + 49-6221-567503; fax: + 49-6221-565258.
E-mail address: michael_scherg@med.uni-heidelberg.de (M. Scherg)

1388-2457/99/$ - see front matter
CLINPH 98740
PII: S1388-2457(98)00056-X

In addition to task and control stimuli experiments, it is of great importance to be able to compare the activation of brain response components that are differentially activated in several related stimuli and cognitive task conditions. All these situations require an appropriate method that can extract signal components which are specific to one condition compared to other conditions.

In this paper, the method of common spatial subspace decomposition (CSSD) is proposed to solve the above problem. This method is based on simultaneous diagonalization of two real symmetric matrices (Fukunaga, 1972; Koles et al., 1990; Koles, 1991; Soong and Koles, 1995) and spatio-temporal source modeling (Scherg and von Cramon, 1985, 1986; Scherg, 1990; Scherg and Picton, 1991; Mosher et al., 1992; Berg and Scherg, 1994). Using CSSD, spatial factors and the corresponding spatial filters, specific to one condition, can be constructed. Target signal components can then be extracted by applying the resulting spatial filters and spatial factors to the original MEG/EEG measurements.

2. Methods

2.1. Spatio-temporal source model

Denote artifact free average referenced multiple channel evoked responses under two conditions as spatio-temporal signal matrices X_A and X_B with dimension of N (channels) by T (samples). For the purpose of convenience, we assume $T > N$. The spatial covariance of the MEG/EEG during these two epochs can then be estimated by

$$R_A = X_A X_A^T, \qquad R_B = X_B X_B^T \tag{1}$$

where X^{T} denotes the transpose of matrix $\boldsymbol{X}$.

The spatio-temporal signal matrices can be modeled using multiple overlapping sources. For the convenience of derivation, we will start by disregarding effects of neglect noise at first. Then X_A and X_B can be modeled as follows:

$$X_A = \begin{bmatrix} C^a \\ C_a \end{bmatrix} \begin{bmatrix} S^a \\ S_A^c \end{bmatrix}, \qquad X_B = \begin{bmatrix} C^b \\ C_c \end{bmatrix} \begin{bmatrix} S^b \\ S_B^c \end{bmatrix} \tag{2}$$

where C^a consists of $\boldsymbol{m_a}$ spatial patterns (column vectors) specific to condition $\boldsymbol{A}$, C_b consists of $\boldsymbol{m_b}$ spatial patterns (column vectors) specific to condition $\boldsymbol{B}$, and C_c consists of $\boldsymbol{m_c}$ spatial patterns (column vectors) common to conditions $\boldsymbol{A}\&\boldsymbol{B}$. Every spatial pattern describes the stationary topographic distribution of a specific source or source configuration at the superficial sensors. S^a, S_A^c , S^b and S_B^c are the corresponding source activity waveforms (row vectors). Note that the source waveforms S_A^c and S_B^c , corresponding to common spatial patterns C^c, are not necessarily the same in the two conditions. Without loss of generality, assume the sources to be linearly independent and

$$K = m_a + m_b + m_c \leq N$$

The aim of our processing is to estimate $C^a S^a$ (or $C^b S^b$) from the data sets X_A and X_B.

2.2. Simultaneous diagonalization of two covariance matrices

The first step of the diagonalization is to factorize the sum covariance matrix of R_A and R_B into the product of eigenvectors and eigenvalues, i.e.

$$R = R_A + R_B = U_0 \cdot \Sigma \cdot U_0^T \tag{3}$$

where U_0 is the matrix of eigenvectors and Σ is the diagonal matrix of the eigenvalues. In subsequent steps, and without special explanation, we take only the components with non–zero singular values into consideration. The whitening transformation matrix is then formed as:

$$P = \Sigma^{-1/2} \cdot U_0^T \tag{4}$$

Now if R_A and R_B are individually transformed as

$$S_A = P \cdot R_A \cdot P^T, \qquad S_B = P \cdot R_B \cdot P^T \tag{5}$$

S_A and S_B exhibit the following two important properties:

1. They share common eigenvectors, i.e.

$$S_A = U \cdot \Sigma_A \cdot U^T, \qquad S_B = U \cdot \Sigma_B \cdot U^T \tag{6}$$

2. The sum of the corresponding eigenvalues for the two matrices will always be 1, i.e.

$$\Sigma_A + \Sigma_B = I \tag{7}$$

Assume that the diagonal elements in Σ_{A} are in descending order, then the variance accounted for by the first several spatial factors are maximal for condition A, and minimal for condition B. Hence, this transformation is optimal for separating the variance in two signal matrices.

2.3. CSSD

The process in Eq. (3) is equivalent to applying principal component analysis (PCA) to the hybrid signal matrix X as follows:

$$X = \left[X_A \vdots X_B \right] = U_0 \cdot \Sigma^{1/2} \cdot V_0^T = U_0 \cdot \Sigma^{1/2} \cdot \left[V_{0A}^T \vdots V_{0B}^T \right] \tag{8}$$

where the dimension of X is $N \times 2T$. According to the assumption in Section 1, the rank of X is K. Therefore, the effective dimensions of matrices U_0, Σ, V_{0A}^T and V_{0B}^T are $N \times K$, $K \times K$, $K \times T$ and $K \times T$, respectively. Note that U_0, Σ here are the same as in Eq. (3).

Denote $\boldsymbol{W}$ as the product of U_0 and $\Sigma^{1/2}$,

$$W = U_0 \Sigma^{1/2} \tag{9}$$

It can be seen that $\boldsymbol{W}$ is the pseudoinverse of the whitening transformation matrix in Eq. (4) and we have

$$X_A = W \cdot V_{0A}^T, \qquad X_B = W \cdot U_0, \Sigma_{0B}^T \tag{10}$$

So $\boldsymbol{W}$ consists of K linearly independent spatial factors (column vector) common to matrices X_A and X_B. Note that V_0 is a (column) orthogonal matrix but V_{0A} and V_{0B} are not. However, similar to S_A and S_B in Eq. (5), V_{0A}^T and V_{0B}^T share the same spatial eigenvectors $\boldsymbol{U}$, i.e.

$$V_{0A}^T = U \cdot \Sigma_A^{1/2} \cdot V_A^T, \qquad V_{0B}^T = U \cdot \Sigma_B^{1/2} \cdot V_B^T \tag{11}$$

where $\boldsymbol{U}$, Σ_A and Σ_B are same as in Eqs. (6) and (7), and V_A and V_B are orthogonal matrices consisting of orthogonal temporal waveforms. Therefore Eq. (8) can be re-written as

$$X = [X_A \quad X_B] = W \cdot U \cdot \left[\Sigma_A^{1/2} \cdot V_A^T \quad \Sigma_B^{1/2} \cdot V_B^T \right]$$
$$= SP \cdot \left[\Sigma_A^{1/2} \cdot V_A^T \quad \Sigma_B^{1/2} \cdot V_B^T \right] \tag{12}$$

where SP is the rotated (W rotated by U) spatial factors common to matrices X_A and X_B. Because the rank of matrix X_A is $(\boldsymbol{m}_a + \boldsymbol{m}_c)$, only the first $(\boldsymbol{m}_a + \boldsymbol{m}_c)$ singular values in the diagonal matrix Σ_A are non–zero. For the same reason, only the last $(\boldsymbol{m}_b + \boldsymbol{m}_c)$ singular values in the diagonal matrix Σ_B are non-zero. Thus Σ_A and Σ_B take the following forms:

$$\Sigma_A = \begin{bmatrix} \overbrace{1 \;\; \ddots \;\; 1}^{m_a} & & & 0 \\ & \overbrace{\sigma_1 \;\; \ddots \;\; \sigma_{mc}}^{m_c} & & \\ & & \overbrace{0 \;\; \ddots \;\; 0}^{m_b} & \\ 0 & & & 0 \end{bmatrix}$$

$$\Sigma_B = \begin{bmatrix} \overbrace{0 \;\; \ddots \;\; 0}^{m_a} & & & 0 \\ & \overbrace{\delta_1 \;\; \ddots \;\; \delta_{mc}}^{m_c} & & \\ & & \overbrace{1 \;\; \ddots \;\; 1}^{m_b} & \\ 0 & & & 0 \end{bmatrix} \tag{13}$$

Therefore, only the middle $\boldsymbol{m}_c$ spatial factors in SP are really common to matrices X_A X_B. The first $\boldsymbol{m}_a$ spatial factors only belong to X_A, and the last $\boldsymbol{m}_b$ spatial factors only belong to X_B. Thus SP consists of three parts:

$$SP = \left[SP^a \quad SP^c \quad SP^b \right] \tag{14}$$

The spatial filters, corresponding to SP, can then be divided into three parts accordingly:

$$SF = U^T \cdot P \begin{bmatrix} SF^a \\ SF^c \\ SF^b \end{bmatrix} \tag{15}$$

Clearly, the spatial subspace spanned by spatial factors SP^c is the same as the spatial subspace spanned by the common spatial patterns C^c in Eq. (2). That means, by the above operation we can extract from matrices X_A and X_B (or covariance matrices R_A and R_B), the common spatial subspace which exists in condition $\boldsymbol{A}$ and condition $\boldsymbol{B}$. Applying CSSD is to decompose the original signal matrices according to above classification of the spatial factor matrix $\boldsymbol{SP}$.

$$X_A = \left[SP^a : SP^c \right] \cdot \begin{bmatrix} TP^a \\ TP_A^c \end{bmatrix}, \; X_B = \left[SP^b : SP^c \right] \cdot \begin{bmatrix} TP^b \\ TP_B^c \end{bmatrix} \tag{16}$$

where TP^a, TP^b, TP_A^c, and TP_A^c are corresponding temporal patterns obtained from Eq. (12) according to the singular value distribution in (13). In CSSD, we take $SP^a * TPa$ (or $SP^b * TPb$) as the estimate of $C^a * Sa$ (or $C^b * Sb$).

The relationship between CSSD and the spatio-temporal source model can be described by Fig. 1 (see proof in Appendix A). In this figure, $\overline{C^c}$ is the spatial subspace spanned by the common spatial patterns C^c , $\overline{\boldsymbol{C^a}}$ is the spatial subspace spanned by spatial patterns C^a , $\overline{\boldsymbol{SP^c}}$ is the spatial subspace spanned by the common spatial factors SP^c from CSSD, $\overline{SP^a}$ is the spatial subspace spanned by the spatial factors SP^a from CSSD, and $\overline{S_A^c}$, $\overline{S^a}$, $\overline{TP_A^c}$, $\overline{TP^a}$ are the corresponding temporal subspaces. The common spatial subspace and specific temporal subspace extracted by CSSD are the same as that in the spatio-temporal source model. On the other hand there is distortion in the specific spatial subspace and common temporal subspace extracted by CSSD. However, if the temporal subspaces $\overline{S_A^c}$, and $\overline{S^a}$ in Eq. (2) are mutually orthogonal, such distortion will disappear. In this case, $SP^a * TPa = \boldsymbol{C^a * Sa}$. In other cases, $SP^a * TPa$ is only an approximation of $C^a * Sa$.

2.4. Summary of the CSSD algorithm

The CSSD algorithm is summarized as follows, based on covariance matrix analysis:

Step 1: Estimate covariance matrices using Eq. (1).

Step 2: Construct whitening transformation matrix $\boldsymbol{P}$ and spatial factor matrix $\boldsymbol{W}$ by Eqs.(3),(4)and(9).

Step 3: Transform covariance matrix R_A into S_A using Eq. (5) and factorize S_A according to Eq. (6).

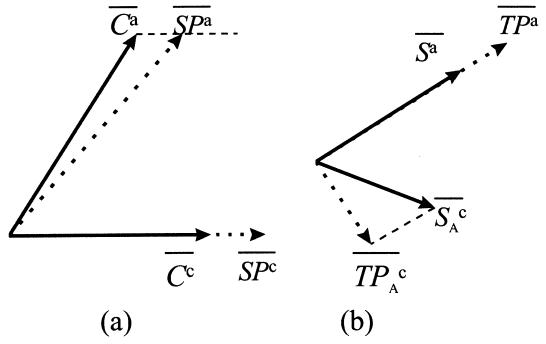

Fig. 1. The relationship between CSSD and spatio-temporal source model: (a) spatial aspect and (b) temporal aspect. $\overline{C^c}$, common spatial subspace; $\overline{C^a}$, specific spatial subspace; $\overline{S_A^c}$, common temporal subspace; $\overline{S^a}$, specific temporal subspace; $\overline{SP^c}$, extracted common spatial subspace; $\overline{SP^a}$, extracted specific spatial subspace; $\overline{TP_A^c}$, extracted common temporal subspace; $\overline{TP^a}$, extracted specific temporal subspace.

Step 4: Take out the first $\boldsymbol{m}_a$ eigenvectors from $\boldsymbol{U}$ (corresponding to the eigenvalues of $\boldsymbol{1}$ in Σ_A). Denote them as U^a . The specific spatial factors are then constructed as

$$SP^a = W \cdot U^a \tag{17}$$

The corresponding spatial filters are

$$SF^a = U^{aT} \cdot P \tag{18}$$

Step 5: Estimate the signal components specific to condition $\boldsymbol{A}$ using the following equation:

$$X_A^a = SP^a \cdot SF^a \cdot X_A \tag{19}$$

For this algorithm, several points must be addressed. First, the covariance matrix is estimated using sample covariance in Eq. (1). Since artifacts and bad channels in practical recordings can change the spatial factor dramatically and thus make the result of CSSD meaningless, the preprocessing should ensure removal of artifacts and rejection of bad channels before applying CSSD. Second, in practical MEG/EEG signal processing, because of the presence of noise, the largest value in Σ_A will be less than $\boldsymbol{1}$. In step 4, $\boldsymbol{m}_a$ should be estimated by finding the turning point of the singular spectrum (see example in Fig. 3b). Third, if there are more than two conditions in practice (say n conditions) and we want to know what is specific to one condition compared to all the other conditions, we can take the covariance matrix for one condition as R_A and the sum of covariance matrices for other $n-1$ conditions as R_B , then apply CSSD to R_A and R_B to extract what we want.

3. Results

3.1. Situation with mutually orthogonal temporal subspaces

The following source model was adopted to conduct the computer simulation.

$$X_A = [c_1 c_2 c_3 c_4] \cdot \begin{bmatrix} s_1 \\ s_2 \\ s_3 \\ s_4 \end{bmatrix}, \qquad X_B = [c_3 c_4 c_5 c_6] \cdot \begin{bmatrix} s_5 \\ s_6 \\ s_7 \\ s_8 \end{bmatrix} \tag{20}$$

where c_i are spatial patterns with dimension of 122×1, and s_i are corresponding source waveforms with dimension of 1×200. c_i are taken from a 122-lead MEG measurement at 6 arbitrary time points, and samples of 6 arbitrary channels during an epoch of 500 ms are used as s_i . (Here, a Neuromag-122™ whole head MEG system was used with a sampling rate of 400 Hz.) Two spatial patterns, c_3 and c_4 , are common to condition A and condition B. To simulate the

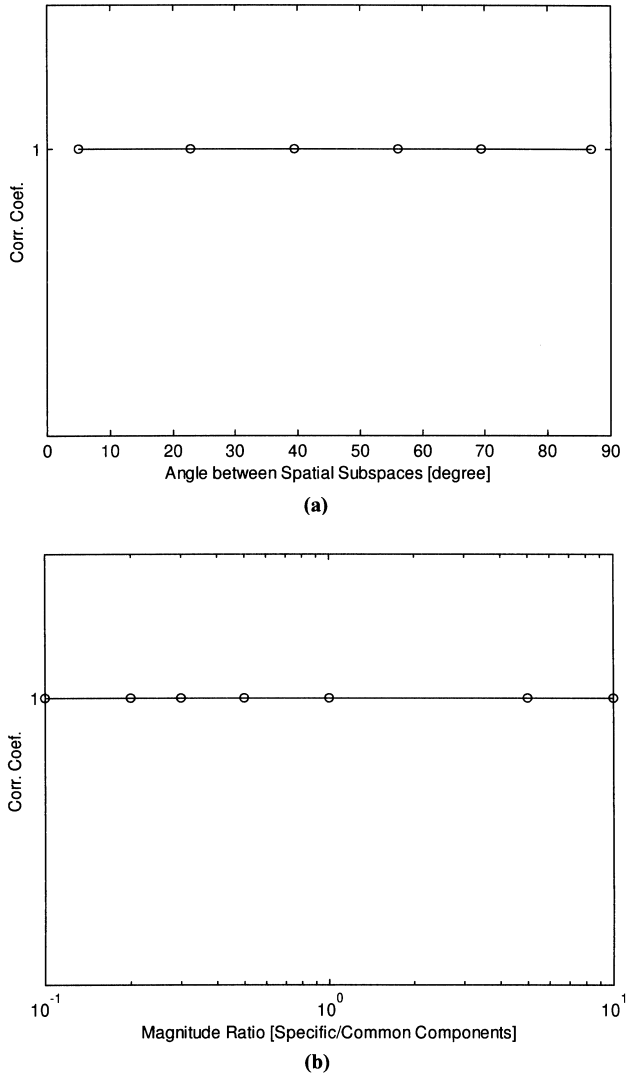

Fig. 2. Decomposing capability of CSSD. The vertical axis is the correlation coefficient between the CSSD-extracted specific part and the actual specific part in X_A . The horizontal axis in (a) represents the angle between the two spatial subspaces and in (b) is the magnitude ratio of the specific to the common component. Temporal subspaces corresponding to specific and common spatial patterns were mutually orthogonal. Note that different components are completely separated by CSSD.

orthogonality between temporal subspaces, the source waveforms in condition A, s_3 and s_4 , were mathematically transformed so that they are orthogonal to s_1 and s_2 . The relations among source waveforms in condition B, $s_5 - s_8$, are arbitrary.

In this simulation, different angles between the spatial subspaces, spanned by $\{c_1, c_2\}$ and by $\{c_3, c_4\}$, were adopted with various relative magnitudes of common and specific components. The resultant X_A and X_B were then subjected to CSSD analysis. Fig. 2 shows the result of decomposition. The vertical axis is the correlation coefficient between $(SP^a{*}TPa)$ and $(C^a{*}Sa)$. The horizontal axis in (a) represents the angle between the two spatial subspaces and that in (b) is the magnitude ratio of specific component to common component. In this 'no noise' situation, the correlation coefficient was always 1, showing that CSSD can separate the common and specific components completely without any distortion. The angle between spatial subspaces and the relative magnitude of the specific and common components have no effect on CSSD results in such cases.

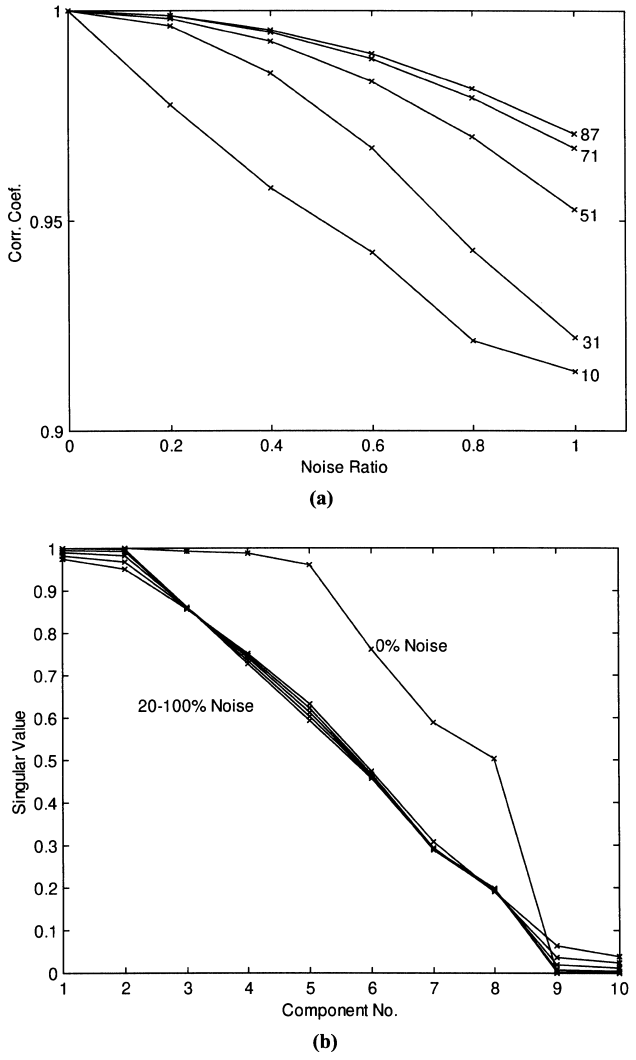

Fig. 3. Effects of noise on CSSD. (a) Noise effect on component separation. The horizontal axis gives the rms amplitude ratio between added GWN and the specific component in the signal matrices. The vertical axis represents the correlation coefficient between CSSD-extracted components and the actual components. Five curves correspond to five different angles between common and specific spatial subspaces in model (20). The angles in degrees are shown to the right of each curve. (b) Singular spectrum in Σ_A under different noise conditions. The horizontal axis represents the component number, and the vertical axis is the singular value. One curve corresponds to the 'no noise' situation, and the other 5 curves correspond to 20, 40, 60, 80 and 100 noise.

Because there exists noise in actual MEG measurement, Gaussian white noise (GWN) was added as sensor measurement noise to the model (20) to simulate a more realistic situation. The effect of GWN on CSSD is shown in Fig. 3a. The horizontal axis gives the root mean square ratio between added noise and specific component in signal matrices, and the vertical axis represents the correlation coefficient between $(SP^a{*}TPa)$ and $(C^a{*}Sa)$. Five curves correspond to five different angles between common and specific spatial subspaces in model (19). The angles in degrees are depicted on the right side of each curve. It is clearly shown that, as the angle between spatial subspaces decreases, the separation result becomes worse. This means that noise affects the spatial resolution of CSSD. However, even if the noise is of the same magnitude as the signal and the angle between common and specific spatial subspaces is as small as 10 degrees, the correlation coefficient between the extracted and actual components is still greater than 0.91.

Fig. 3b gives one example of the singular spectrum in Σ_A. As stated in Section 2, if there is no noise, the components specific to condition A have the singular value of 1 in Σ_A. If the noise is not zero, the largest value in Σ_A is less than 1 (see the curves in the figure with 20–100% noise). By finding the turning points of these curves, the first two components were selected as specific to condition A, which is consistent with the current model. In this figure, the rank of the whitening transformation matrix was selected as 10.

The above results demonstrate that CSSD provides excellent decomposition for common and specific sources if there is no temporal correlation between specific and common sources.

3.2. Situation with mutually NON-orthogonal temporal subspaces

In realistic situations, the temporal subspaces spanned by S^a and S_A^c are unlikely to be mutually orthogonal. Such a situation was simulated in the model (20) by changing the angle between the subspace spanned by source waveforms s_3 , s_4 , and that spanned by source waveforms s_1 and s_2 . The result of CSSD applied to such case is shown in Fig. 4. The horizontal axis represents the correlation coefficient between $\{s_1, s_2\}$ and $\{s_3, s_4\}$. The vertical axis is the correlation coefficient between $(SP^a{*}TPa)$ and $(C^a{*}Sa)$. Fig. 4a is the result for the no noise situation and Fig. 4b is the result when 15% white noise was added to each sensor. The strength of the noise is defined as the root mean square

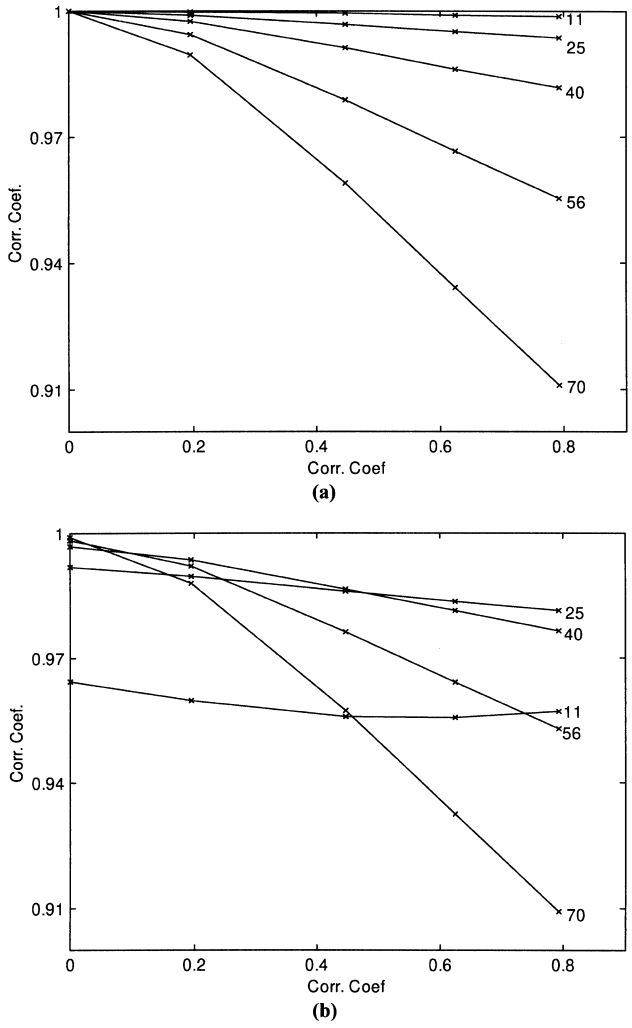

Fig. 4. Effects of non-orthogonality between temporal subspaces on CSSD: (a) 'no noise', and (b) 15% noise. The horizontal axis is the correlation coefficient between source waveforms corresponding to specific and common spatial patterns. The vertical axis is the correlation coefficient between the CSSD extracted specific part and the actual specific part in X_A . Five curves correspond to 5 different angles between common and specific spatial subspaces in model (20), and the angles in degrees are shown to the right of each curve. The effect of temporal correlation decreases as the angle between spatial subspaces decreases, and the combined effect of temporal correlation and noise gives rise to the result in (b).

ratio between added noise and the signal. The five curves correspond to five different angles between common and specific spatial subspaces in model (20). The angles in degrees are depicted on the right side of each curve in the figures. Note that the effect of temporal correlation decreases as the angle between spatial subspaces decreases (Fig. 4a), and the combined effect of temporal correlation and noise (see Fig. 3a) gave rise to the result in Fig. 4b. It is shown that, even when the correlation coefficient between $\{s_1, s_2\}$ and $\{s_3, s_4\}$ is as high as 0.8, CSSD can still give a good extraction of the specific component with a correlation coefficient of more than 0.94 for most cases.

3.3. Simulation based on dipole sources

In order to test the efficiency of source extraction by CSSD, further simulations based on BESA® (MEGIS Software GmbH, Munich) were conducted. Multiple temporally overlapping current dipoles located within a single-shell spherical head model (Sarvas, 1987) were adopted to model sources of brain activity. MEG forward solutions were used to simulate measured data sets, and 122 sensors (Neuromag-122®) were used for the forward solution. Two kinds of noise, spatially correlated and uncorrelated, were considered in this simulation. The correlated noise was simulated by several additional dipole sources, and the uncorrelated noise was simulated by adding 15% white noise to each sensor. The noise strength is defined as the root mean square ratio between added noise and the forward solution.

Fig. 5 shows one example of the source models for the simulated condition *A* and condition *B*. In condition *A*, 5 dipole sources were activated, while only sources 3–5 were activated in condition *B*. Source 5 was used to represent

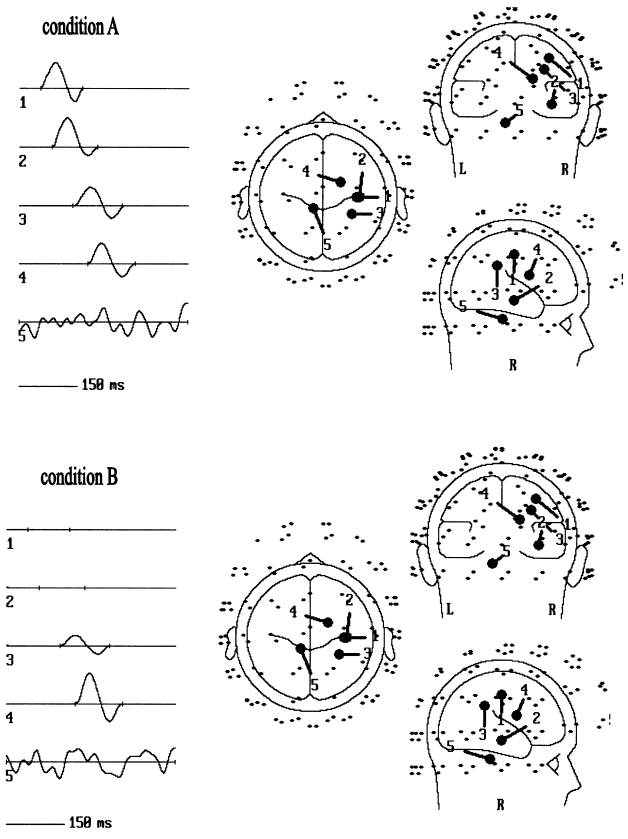

Fig. 5. Simulated source models. In condition *A*, 5 sources were activated. The source waveform for each source is depicted on the left and labeled with the same number as in the head model. Three projections of the head model with the MEG sensors configuration are shown on the right. In condition *B*, only the common sources 3–5 were activated. In both conditions, source 5 was used to simulate the spatially correlated noise and 15% white noise was added to each sensor as measurement noise. Note that there is low correlation between common and specific sources in condition *A*.

Table 1
Correlation coefficients between different sources (spatial/temporal)

	Source 1	Source 2
Source 3	0.50/0.05	0.01/0.21
Source 4	0.35/0.03	0.76/0.05
Source 5	0.03/0.00	0.06/0.00

correlated noise (the frequency band of noise is 0–25 Hz). Therefore, sources 1 and 2 are specific to condition *A*, and sources 3–5 are common to both conditions. The correlation coefficients between specific and common sources are listed in Table 1. Note that there is no temporal correlation between source 5 and any of the other sources.

The simulated data sets, generated as above, were processed using CSSD, and the extracted signal components specific to condition *A* was then analyzed using BESA®. Fig. 6a shows the result of brain source imaging (i.e. imaging source activity) using the same 5 dipole sources as in Fig. 5. We can see that source waveforms for sources 1 and 2 were accurately extracted by CSSD. Because common and specific sources were temporally correlated, sources 3 and 4 exhibit a small residual activity. Note that, because the specific temporal subspace can be extracted without any distortion, the residual sources 3 and 4 were only active within the epoch of time when source 1 and 2 were active. Because there was no temporal correlation between source 5 and the specific sources, there was no residual spatial component for this source.

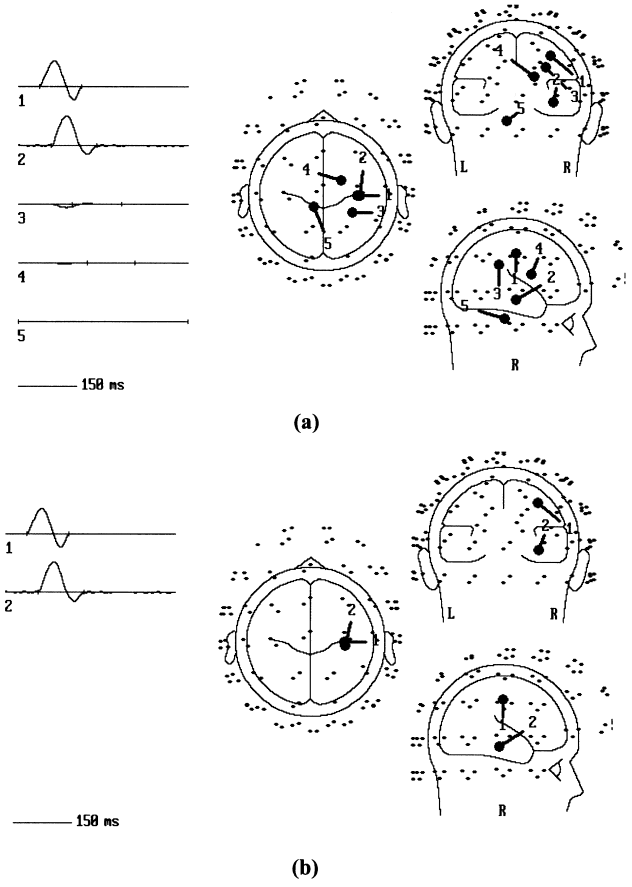

Fig. 6. Result of CSSD applied to the simulated situation: (a) using the same source configuration as in Fig. 5, and (b) using spatio-temporal source analysis to fit a two-dipole source model. Sources 1 and 2, specific to condition A, were extracted very accurately by CSSD. Because the temporal correlation between different sources was low, the spatial distortion, represented by small components of sources 3 and 4, is negligible in this case.

The extracted signal components specific to condition *A* were also subjected to spatio-temporal source analysis using a two-dipole model (Fig.6b). The resulting waveforms of sources 1 and 2 were very similar to the original simulation, except for some added noise. However, locations deviated from actual source locations of sources 1 and 2 by 0.13 ± 0.06 mm and 2.03 ± 0.44 mm, respectively. Here, the standard deviation is due to white noise.

Fig. 6 also indicates that the spatially correlated noise of the common source 5, could be largely removed by CSSD from the specific source components.

In the above example, the temporal correlation between common and specific sources is relatively low. To test the effects of different temporal correlation on source extraction by CSSD, we changed the onset time of (common) source 3 while keeping all the other sources unchanged, so that the correlation coefficient between source 3 and the specific sources (1 and 2) varied. In every case, the resulting waveforms of sources 1 and 2 were similar to the original simulation, while the location deviations differed. Table 2 gives the results of the location deviation for two-dipole spatio-temporal fitting under different temporal correlation conditions. It is shown that for low temporally correlated sources, CSSD can provide a good source extraction, while the spatial distortion is serious for highly temporally correlated sources. Note that these deviations are the summed effects of the spatial distortion and the 15% white noise added in the simulated measurements.Fig. 7 gives a more realistic example with two pairs of bilateral sources. The source models for conditions *A* and *B* are shown in Fig. 7a. There were 7 dipole sources in total, of which sources 5–7 were used to represent spatially correlated noise signals. In condition *A*, all the sources were activated while only sources 3–7 were activated in condition *B*. Compared to condition *A*, source 3 had reduced magnitude of activity in condition *B*, and source 4 was delayed in onset time. The spatial and temporal correlation between different sources in condition *A* is listed in Table 3. Note that all the sources are temporally correlated. In addition to source activities, 15% white noise was added to every sensor to simulate the measurement noise. The separation result of CSSD is shown in Fig. 7b, using the same source model as in (a). The effect of temporal correlation on source separation is clearly shown in (b), i.e. there are residual activities for common sources 3–7 because there are temporal correlations between common and specific sources. Note that the residual activation waveform of every common source is a

Table 2
Location deviation under different temporal correlation conditions

Correlation coefficient between Source 3 and		Location deviation (mm)	
Source 1	Source 2	Source 1	Source 2
0.00	0.00	0.09 ± 0.09	0.52 ± 0.27
0.03	0.10	0.12 ± 0.06	0.70 ± 0.47
0.05	0.21	0.13 ± 0.06	2.03 ± 0.44
0.10	0.38	0.52 ± 0.05	3.53 ± 0.21
0.15	0.54	0.64 ± 0.07	4.74 ± 0.23
0.19	0.69	0.84 ± 0.05	5.57 ± 0.19
0.24	0.82	1.04 ± 0.04	6.19 ± 0.16

linear combination of sources 1 and 2, so the active epochs of time of common sources in (b) were different from those in (a).

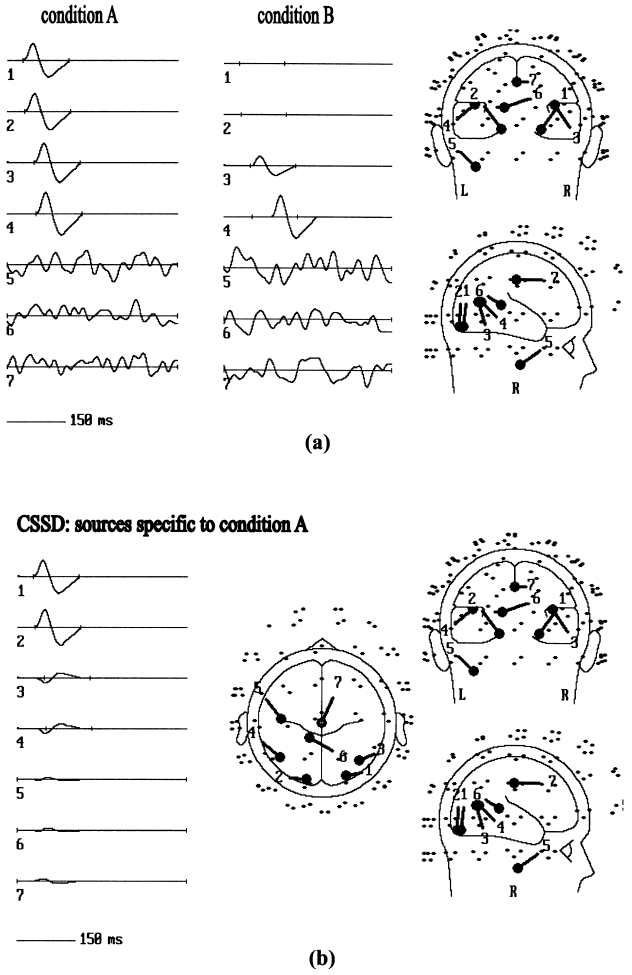

Fig. 7. Simulation for bilateral sources: (a) source models of two conditions, and (b) result of CSSD. Seven sources were activated in condition *A*, and only sources 3–7 were activated in condition *B*. Sources 5–7 were used to represent spatially correlated noise, and sources 3 and 4 were activated differently in the two conditions. The result extracted by CSSD contains the complete spatial and temporal information about sources 1 and 2. Because of the temporal correlation between common and specific sources, there were residual spatial components of the common sources.

3.4. Applied to multiple task conditions

To test the efficiency of CSSD in analyzing multiple task conditions, 3 conditions were simulated based on BESA®. Fig. 8a shows source models of 3 conditions. From left to right, columns 1–3 represent conditions 1, 2, and 3, respectively. Condition 1 is exactly the same as condition *A* in Fig. 5a, while sources 3 and 5 were activated in condition 2, and sources 4 and 5 were activated in condition 3. Thus, only sources 1 and 2 are specific to condition 1. From the simulated measurements X_1, X_2, and X_3, two covariance matrices can be estimated as

$$R_A = X_1 \cdot X_1^T, \qquad R_B = X_2 \cdot X_2^T + X_3 \cdot X_3^T$$

By applying steps 2–5 of the CSSD algorithm, the components specific to condition 1 can be extracted (see Fig. 8b). The result is exactly the same as that in Fig. 6a, showing that CSSD can be applied to multiple conditions to extract what is specific to one condition compared to all the other conditions.

4. Discussion

We have proposed a method that can extract signal components specific to one condition from multiple MEG/EEG data sets of multiple task conditions. The proposed method is based on dissociation of the spatial subspaces common and specific to each condition. The relationship between this decomposition and spatio-temporal source models was described in both spatial and temporal domains. Computer simulations have demonstrated the validity and effectiveness of this method.

Simultaneous diagonalization of two real symmetric matrices (Fukunaga, 1972) has previously been used by Koles et al. (1990), Koles (1991) and Soong and Koles (1995), in order to extract abnormal components from clinical EEG. In this process, a spatial filter was constructed from Eqs. (3)–(7) as

$$F = U^T \cdot P \tag{21}$$

The original EEG was transformed into uncorrelated components by

$$Z = F \cdot X_A \tag{22}$$

The components in Z were then visually reviewed by EEG experts and the components that were thought to be abnormal, for example with spike and sharp waves, were selected to reconstruct the EEG. Such extraction is a kind of a blind separation because an exact relationship between extracted components and actual abnormal components is not defined. The main innovation in CSSD is that the relationship between the diagonalization and the underlying source models is revealed and the common spatial subspace is used as the basis for component separation. Therefore,

Table 3
Correlation coefficients between different sources (spatial/temporal)

	Source 1	Source 2	Source 3	Source 4	Source 5	Source 6	Source 7
Source 1	1/1	–	–	–	–	–	–
Source 2	0.30/0.95	1/1	–	–	–	–	–
Source 3	0.15/0.48	0.19/0.50	1/1	–	–	–	–
Source 4	0.09/0.45	0.20/0.48	0.09/0.95	1/1	–	–	–
Source 5	0.08/0.01	0.24/0.03	0.05/0.08	0.20/0.06	1/1	–	–
Source 6	0.13/0.04	0.06/0.07	0.29/0.12	0.63/0.17	0.30/0.23	1/1	–
Source 7	0.02/0.11	0.14/0.11	0.19/0.17	0.24/0.16	0.09/0.23	0.23/0.13	1/1

CSSD has the advantage that components are separated according to their spatial patterns.

Another innovation in CSSD is that the temporal relationship between different sources is included. The main limitation is that, if the common source waveforms S_A^c and specific source waveforms *Sa* are correlated, there will be a distortion in the extracted specific spatial patterns SP^a . Although simulation results (Figs. 4 and 6b) show that such distortion is not a serious problem if the temporal correlation is low, correction would be needed in situations where precise spatial patterns are crucial, for example, to distinguish highly correlated sources (cf. Table 2 and Fig. 7). One possible way to correct SP^a is to combine CSSD and source analysis. We can see in Fig. 1 that SP^a is distorted in the direction of the common spatial subspace. This means that there is a residual of the common spatial subspace in SP^a . By source analysis, we could obtain sources corresponding to such a residual (like sources 3–7 in Fig. 7b). Because the common spatial subspace can be extracted exactly, the related sources can be excluded by checking whether the spatial topographies they generated lie in the common spatial subspace. Thus, the distortion to the specific spatial subspace can be removed. For example, the residual sources 3–7 in Fig. 7b lie in the common spatial subspace, so the spatial components corresponding to these sources can be excluded. In this way, the spatial distortion of sources 1 and 2 could be corrected.

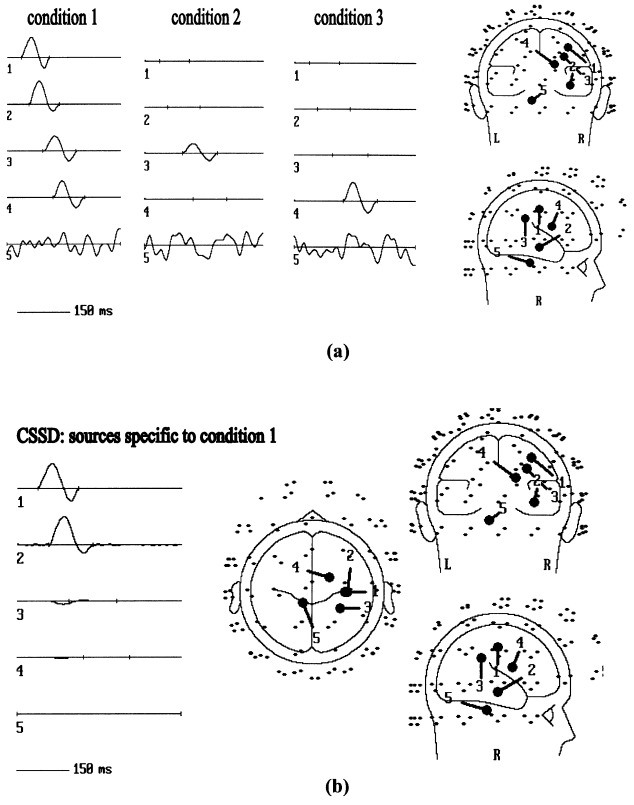

Fig. 8. Simulation for multiple task conditions: (a) source models of three conditions and (b) the extracted result, showing that CSSD is able to extract the complete spatial and temporal information about the sources specific to condition 1.

An interesting application of CSSD is to extract evoked responses from background spontaneous activities. In this case, one data set is obtained from the prestimulus epoch, and the other from the poststimulus epoch that contains the signal information of interest. In most cases, evoked responses and background activities can be assumed to be highly uncorrelated. A study on this topic is in preparation.

When applying CSSD to EEG analysis, it is important to bear in mind that CSSD is different from other spatial filtering methods like surface Laplacian (Hjorth, 1975; Babiloni et al., 1997). The latter can be used to make the EEG signal independent from the reference and improve the spatial details of the potential distribution. CSSD, however, is to separate different (specific and common) brain activities which are overlapped in the scalp measurement. If necessary, surface Laplacian can be applied in cascade with CSSD. Because of the linearity of the Laplacian and CSSD operators, surface Laplacian can be applied either before or after using CSSD.

For experiments employing task and control stimuli, another possible way to extract the information about the target activities is to calculate the difference between covariance matrices from two measurements (Sekihara et al., 1997). However, in addition to requiring uncorrelated specific and common source components, this method would require the temporal waveforms of the common sources to remain the same in the two conditions. In addition, when the control stimulus elicits some activities that do not appear in the task condition, the covariance difference matrix will contain information about such activities in addition to the

information on target activities. Thus, the method is not good for separation of the activities specific to the target condition. CSSD can avoid such difficulties, since the changes in source waveforms (either in latency or amplitude (do not affect the result. of CSSD. In addition, the extracted specific components only contain the information about the target activities.

For multiple conditions, the method proposed in this paper is a simplified way to extract components specific to one condition compared to all the other conditions. Our results demonstrate that this may be an efficient approach. A possible way to fully analyze multiple conditions is to compare the covariance matrices of N conditions in a pairwise fashion. In this approach, in addition to $N(N-1)/2$ comparisons, further processes must be taken to extract an optimal spatial filter from the multiple comparisons. If the comparison between every 2 conditions is not of interest, the presented simplified approach is a feasible first step.

Combining all the advantages discussed above, our results suggest that CSSD merits further development and application.

Acknowledgements

This work is supported by The Alexander von Humboldt Foundation. We wish to thank Nicole Ille for her helpful comments on the manuscript.

Appendix A. Relationship between CSSD and the spatio-temporal source model

During the PCA procedure, the spatial subspaces remain unchanged, therefore

$$\text{span}\{SP^a \quad SP^c\} = \{c^a \quad c^c\}$$

$$\text{span}\left\{SP^b \quad SP^c\right\} = \left\{c^b \quad c^c\right\}$$

therefore

$$\text{span}\{SP^c\} = \{C^c\} \tag{A.1}$$

Using *CSSD*, we can obtain the spatial filters, SF^a and SF^c, corresponding to SP^a and SP^c, respectively, such that $SF^a \cdot SP^c = 0, \quad SF^c \cdot SP^a = 0$

Therefore $SF^a \cdot C^c = 0$

and

$$TP^a = SF^a \cdot X_A = SF^a \cdot \left[C^a : C^c\right] \cdot \begin{bmatrix} S^a \\ S_A^c \end{bmatrix} = (SF^a \cdot C^a) \cdot Sa$$

$$\Rightarrow \text{span}\{TP^a\} = \text{span}\{S^a\} \tag{A.2}$$

Because of the orthogonality between TPa and TP_A^c, it is straightforward to obtain the relation that the temporal subspace spanned by TP_A^c is the projection from the subspace spanned by S_A^c to the zero-space of the subspace spanned by Sa.

Also because of the orthogonality between TPa and TP_A^c, we have

$$SP^a = X_A \cdot TPa^T = C^a \cdot (S^a \cdot TP^{aT}) + C^c \cdot (S_A^c \cdot TP^{aT}) \tag{A.3}$$

That is, the spatial subspace spanned by SPa is the same as the subspace spanned by Ca with distortion in the direction of Cc. Such distortion depends on the correlation between S_A^c and Sa. When S_A^c is orthogonal to Sa, the distortion will disappear (the second term on the right-hand side of Eq. (A.3) becomes zero).

References

Aine C, Supek S, George J, Ranken D, Best E, Tiee W, Vigil V, Flynn E, Wood C. MEG studies of human vision: retinotopic organization of V1. In: C. Baumgartner et al. (Eds.), Biomagnetism: Fundamental Research and Clinical Applications. Amsterdam: Elsevier, 1995;153–161.

Babiloni F, Babiloni C, Carducci F, Del Gaudio M, Onorati P, Urbano A. A high resolution EEG method based on the correction of the surface Laplacian estimate for the subject's variable scalp thickness. Electroenceph clin Neurophysiol 1997;103:486–492.

Beisteiner R, Huter D, Edward V, Koch G, Franzen P, Egkher A, Lindinger G, Baumgartner C, Lang W. Brain potentials with old/new distinction of non-words and geometric figures. Electroenceph clin Neurophysiol 1996;99:517–526.

Berg P, Scherg M. A multiple source approach to the correction of eye artifacts. Electroenceph clin Neurophysiol 1994;90:229–241.

Elbert T, Rockstroh B, Kowalik ZJ, Hoke M, Molnar M, Skinner JE, Birbaumer N. Chaotic brain activity. Electroenceph clin Neurophysiol Suppl 1995;44:441–449.

Fukunaga K. Introduction to statistical pattern recognition. New York: Academic Press, 1972.

Gevins A, Smith ME, Le J, Leong H, Bennett J, Martin N, McEvoy L, Du R, Whitfield S. High resolution evoked potential imaging of the cortical dynamics of human working memory. Electroenceph clin Neurophysiol 1996;98:327–348.

Hämäläinen M, Hari R, Ilmoniemi RJ, Knuutila J, Lounasmaa OV. Magnetoencephalography-theory, instrumentation, and applications to noninvasive studies of the working human brain, Rev Mod Phys 1993;65:413–497.

Hjorth B. An online transformation of EEG scalp potentials into orthogonal source derivations. Electroenceph clin Neurophysiol 1975;39:526–530.

Koles ZJ. The quantitative extraction and topographic mapping of the abnormal components in the clinical EEG. Electroenceph clin Neurophysiol 1991;79:440–447.

Koles ZJ, Lazar MS, Zhou Z. Spatial patterns underlying population differences in the background EEG. Brain Topogr 1990;2:275–284.

Lehmann D, Michel CM, Pal I, Pascual-Marqui RD. Event-related potential maps depend on pre-stimulus brain electric microstate map. Int J Neurosci 1994;74:239–248.

Mosher JC, Lewis PS, Leahy RM. Multiple dipole modeling and localization from spatio-temporal MEG data. IEEE Trans Biomed Eng 1992;39:541–557.

Nunez PL. Electric fields of the brain, New York: Oxford University Press, 1981.

Rossini PM, Deuschl G, Pizzella V, Tecchio F, Pasquarelli A, Feifel E, Romani GL, Lucking CH. Topography and sources of electromagnetic

cerebral responses to electrical and air-puff stimulation of the hand. Electroenceph clin Neurophysiol 1996;100:229–239.

Sasaki K, Tsujimoto T, Nambu A, Matsuzaki R, Kyuhou S. Dynamic activities of the frontal association cortex in calculating and thinking. Electroenceph clin Neurophysiol 1989;74:58–75.

Sarvas J. Basic mathematical and electromagnetic concepts of the biomagnetic inverse problem. Phys Med Biol 1987;32:11–22.

Scherg M. Fundamentals of dipole source potential analysis. In: Grandori F, Hoke M, Romani GL, editors. Auditory evoked magnetic fields and electric potentials (Advances in audiology, Vol. 6). Basel: Karger, 1990:40-69.

Scherg M, Picton TW, Separation and identification of event–related potential components by brain electric source analysis. In: Brunia CHM Mulder G, Verbaten MN, editors. Event-related potentials of the brain (EEG Suppl. 42). Amsterdam: Elsevier, 1991:24–37.

Scherg M, von Cramon D. Two bilateral sources of the late AEP as identified by a spatio-temporal dipole model. Electroenceph clin Neurophysiol 1985;62:32–44.

Scherg M, von Cramon D. Evoked dipole source potentials of the human auditory cortex. Electroenceph clin Neurophysiol 1986;65:344–360.

Sekihara K, Poeppel D, Marantz A, Phillips C, Koizumi H, Miyashita Y. MEG covariance difference analysis: extraction of target source activities by using task and control measurement. NeuroImage 1997; 5(Suppl.):444.

Soong ACK, Koles ZJ. Principal-component localization of the sources of the background EEG. IEEE Trans Biomed Eng 1995;42:59–67.

Srebro R, Ogui RM. Estimating cortical activity from VEPS with the shrinking ellipsoid inverse. Electroenceph clin Neurophysiol 1997; 102:343–355.